NicE-C efficiently reveals open chromatin–associated chromosome interactions at high resolution

Zhengyu Luo,[1,7] Ran Zhang,[2,7] Tengfei Hu,[3,7] Yuting Zhu,[3] Yueming Wu,[3] Wenfei Li,[4] Zhi Zhang,[5] Xuebiao Yao,[6] Haiyi Liang,[2] and Xiaoyuan Song[1,3]

[1]Department of Urology, the First Affiliated Hospital of University of Science and Technology of China, Division of Life Sciences and Medicine, University of Science and Technology of China, Hefei, Anhui, 230001, China; [2]CAS Key Laboratory of Mechanical Behavior and Design of Materials, Department of Modern Mechanics, University of Science and Technology of China, Hefei, Anhui, 230027, China; [3]MOE Key Laboratory for Cellular Dynamics, CAS Key Laboratory of Brain Function and Disease, School of Life Sciences, Division of Life Sciences and Medicine, University of Science and Technology of China, Hefei, Anhui, 230027, China; [4]Affiliated Psychological Hospital of Anhui Medical University, Hefei Fourth People's Hospital, Anhui Mental Health Center, Hefei, Anhui, 230022, China; [5]CAS Key Laboratory of Brain Function and Disease, School of Life Sciences, Division of Life Sciences and Medicine, University of Science and Technology of China, Hefei, Anhui, 230027, China; [6]MOE Key Laboratory for Cellular Dynamics, University of Science and Technology of China, Hefei, Anhui, 230027, China

Enhancer–promoter communication is known to regulate spatiotemporal dynamics of gene expression. Several methods are available to capture enhancer–promoter interactions, but they either require large amounts of starting materials and are costly, or provide a relative low resolution in chromatin contact maps. Here, we present nicking enzyme-assisted open chromatin interaction capture (NicE-C), a method that leverages nicking enzyme–mediated open chromatin profiling and chromosome conformation capture to enable robust and cost-effective detection of open chromatin interactions at high resolution, especially enhancer–promoter interactions. Using TNF stimulation and mouse kidney aging as models, we applied NicE-C to reveal characteristics of dynamic enhancer–promoter interactions.

[Supplemental material is available for this article.]

Enhancers and promoters are key *cis*-regulatory elements located at open chromatin regions, which can be detected by open chromatin profiling methods, such as FAIRE-seq (Giresi and Lieb 2009), DNase-seq (Song and Crawford 2010), ATAC-seq (Buenrostro et al. 2013), and nicking enzyme-assisted sequencing (NicE-seq) (Ponnaluri et al. 2017). Long-range chromatin interactions between enhancers and promoters can control cell type– and condition-specific gene expression, which play important roles in diverse biological processes, including neural development (Bonev et al. 2017), cell differentiation (Isoda et al. 2017), and etiopathology of diseases (Hua et al. 2018). The development of chromosome conformation capture (3C)-based methods, including Hi-C (Lieberman-Aiden et al. 2009; Rao et al. 2014) and Micro-C (Hsieh et al. 2020; Krietenstein et al. 2020), has greatly promoted our understanding of high-order chromatin organization and enhancer–promoter interactions. However, these genome-wide methods need extremely deep sequencing to provide sufficient spatial resolution to identify enhancer–promoter interactions.

To enrich *cis*-regulatory elements–associated chromatin interactions, especially between enhancers and promoters, methods such as Capture Hi-C (Mifsud et al. 2015), OCENA-C (Li et al. 2018), and Trac-looping (Lai et al. 2018) have been developed. Although Capture Hi-C can identify genome-wide chromatin interactions associated with both active and inactive promoters, it requires a costly, species-specific predesigned biotinylated RNA bait library to target known promoters. OCEAN-C and Trac-looping are probe-free methods that use open chromatin features. OCEAN-C combines Hi-C with FAIRE-seq to select open chromatin interactions, whereas Trac-looping uses transposase enzyme and a bivalent ME linker. Although potentially very promising, Trac-looping requires about 100 million (M) cells per experiment, yet identifies only a relatively low fraction of long-range (>20 kb) *cis* chromatin interactions. Limitation of OCEAN-C falls in its relative lower resolution and lower enrichment of open chromatin regions. Accordingly, an improved method for capturing open chromatin interactions would be highly desirable. To address these challenges, we developed a new probe-free method named nicking enzyme-assisted open chromatin interaction capture (NicE-C) for capturing open chromatin interactions.

Results

To enrich enhancer–promoter interactions in a probe-free way, we attempt to select open chromatin–associated chromatin interactions via combining in situ Hi-C (Rao et al. 2014) with open chromatin profiling method NicE-seq (Ponnaluri et al. 2017), making full use of its limited starting materials requirement and great applicability for fixed cells. In NicE-seq, a sequence-specific nicking

[7]These authors contributed equally to this work.
Corresponding author: songxy5@ustc.edu.cn
Article published online before print. Article, supplemental material, and publication date are at https://www.genome.org/cgi/doi/10.1101/gr.275986.121.

32:534–544 Published by Cold Spring Harbor Laboratory Press; ISSN 1088-9051/22; www.genome.org

enzyme Nt.CviPII (recognizing CCD, D = A/G/T) and *Escherichia coli* DNA polymerase I are used to label open chromatin regions with biotin (Ponnaluri et al. 2017). The nicking enzyme–mediated labeling of open chromatin regions also results in chromatin fragmentation at the same time, and the chromatin ends were not limited to CCD (Supplemental Fig. S1A,B; Ponnaluri et al. 2017). We found that using Nt.CviPII and *E. coli* DNA polymerase I for digesting chromatin instead of using restriction enzyme in Hi-C could simultaneously detect chromatin accessibility and chromatin interactions at high resolution (1 kb) (Fig. 1A–D). Thus, we developed nicking enzyme-assisted open chromatin interaction capture (NicE-C), a method that combines nicking enzyme–mediated chromatin fragmentation in NicE-seq and proximity-based chromatin ends ligation in in situ Hi-C to specifically capture open chromatin region interactions. The overall procedure of NicE-C is similar to that of in situ Hi-C (Fig. 1A), which begins with cutting cross-linked chromatin at open regions by the nicking enzyme Nt.CviPII and *E. coli* DNA polymerase I, chromatin ends are then repaired, followed by bridge linker ligation to capture open chromatin interactions (Fig. 1A).

We first performed NicE-C with approximately 1 million (M) HeLa cells. We found that both of the chromatin accessibility (open chromatin) part and chromatin interaction part of NicE-C were highly reproducible between biological replicates (Supplemental Fig. S1C,D). We then compared NicE-C with NicE-seq data generated in-house and published ATAC-seq data (Cho et al. 2018) for HeLa cells. The results showed that NicE-C efficiently captured open chromatin as evidenced by signal enrichment around both promoters and enhancers, highly similar to that of NicE-seq (Fig. 1B; Supplemental Fig. S1E), and ∼74.2% and 82.1% of called peaks from NicE-C data overlapped with open peaks identified from ATAC-seq and NicE-seq data, respectively (Fig. 1C). We found that the NicE-C data showed strong signal enrichment around previously reported ATAC-seq and DNase-seq peak regions, and the distribution of open chromatin peaks identified by NicE-C was similar to that from the ATAC-seq and DNase-seq data sets (Supplemental Fig. S1F,G). We next evaluated the capacity of NicE-C to capture chromatin interactions compared to the in situ Hi-C data for HeLa cells and to the published Micro-C data for H1-hESC cells (Krietenstein et al. 2020). NicE-C revealed chromatin organization—including A/B compartments, TADs, and chromatin loops—similar to in situ Hi-C and Micro-C (Supplemental Fig. S2A,B, S3A–C). In addition, NicE-C was able to capture fine-scale enhancer–promoter and promoter–promoter interactions (E-P/P-P loops), similar to those detected with Micro-C (Hsieh et al. 2020; Krietenstein et al. 2020), but inefficiently with in situ Hi-C (Fig. 1D–F; Supplemental Fig. S2C, S3D). The heatmaps indicated that NicE-C detects E-P/P-P interactions with sharp and robust signal that are obviously distinct from the unclear interaction signals in the heatmaps depicting the high-resolution Hi-C data (Supplemental Fig. S2C). NicE-C could detect E-P/P-P loops with much less sequencing depth compared to Micro-C (Supplemental Fig. S3D), because NicE-C specifically captures open chromatin interactions. We found that although NicE-C identified A/B compartments that were highly similar to the Hi-C result, the E-P/P-P loops were mostly located in the A compartment; the B compartment without open chromatin peaks did not have E-P/P-P loops (Supplemental Fig. S4A). Next, we compared the major classes of high confidence interactions identified with NicE-C and in situ Hi-C in HeLa cells. The majority (68.5%) of high confidence NicE-C interactions connected *cis*-regulatory elements (P-P, E-P, and E-E), versus 22.1% of in situ Hi-C interactions (Supplemental Fig. S4B). These data showed NicE-C method is robust and reproducible, and the NicE-C method can efficiently capture open chromatin interactions at high resolution.

Having established that NicE-C can effectively capture open chromatin interactions, we next used NicE-C to analyze human lung fibroblast cells (IMR-90) and cells from kidneys of adult female mice to explore the general applicability of NicE-C. As expected, the peaks identified by NicE-C were highly enriched at promoter and enhancer regions (Supplemental Fig. S5A,B). As with HeLa cells, our NicE-C revealed clear enrichment of open chromatin interactions including E-P and P-P loops in IMR-90 and kidney cells (Supplemental Fig. S6). We observed lines extending between E-P/P-P loops in our NicE-C heatmaps and genome-wide averaged pile-up plots for all cell types (HeLa, IMR-90, and kidney cells) we examined (Fig. 1D–F; Supplemental Fig. S6), which correspond to "stripes" thought to result from the process of loop extrusion (Hsieh et al. 2020). The loop extrusion model explains the formation of TADs, "loops" or "dots" and "stripes" or "flames," in chromatin contacts maps (Fudenberg et al. 2016; Banigan et al. 2020). In the loop extrusion process, once loaded onto chromatin, the *cis*-acting loop-extruding factors, such as cohesin, could lead to the formation and enlargement of DNA loops that are stalled by boundary elements, which often are bound by CTCF (Fudenberg et al. 2016). A stripe emerges when one side of extruding is stalled by CTCF while the other side continues extruding (Banigan et al. 2020).

We further divided the enhancers and promoters of HeLa cells into four types based on whether they are overlapped with CTCF or TAD boundaries. The data showed that the E-P/P-P loops or stripes were stronger between enhancers and promoters overlapped with CTCF-bound TAD boundaries (Supplemental Fig. S7A,B), which were much weaker between enhancers and promoters overlapped with neither CTCF nor TAD boundaries (Supplemental Fig. S7A,B). These results indicated that E-P interactions occur in the process of loop extrusion, which can be enhanced by CTCF and/or TAD boundaries. Previous studies have reported that fine-scale E-P/P-P loops and stripes are functionally associated with transcription (Hsieh et al. 2020). To validate this we performed RNA-seq to correlate gene expression to E-P/P-P interactions in HeLa cells. The results showed that the E-P loops and stripes in our NicE-C data were highly correlated with transcription activities, where stronger interactions occurred between enhancers and promoters of higher expressed genes (Supplemental Fig. S8A). This was almost invisible from the Hi-C data (Supplemental Fig. S8B).

We next compared NicE-C with Trac-looping and OCEAN-C. We first compared random convection of chromatin by identifying pairs between genomic DNA and mitochondrial DNA, which are not deemed to interact with each other under normal conditions (Rao et al. 2014). The N_{nm} (reads consisting of genomic DNA and mitochondrial DNA)/N_{total} (total reads) of Trac-looping and OCEAN-C were ∼35-fold and ∼threefold higher than NicE-C, respectively (Supplemental Fig. S9A), indicating that NicE-C minimized the artifacts from diffusion of fragmented chromatin compared with the other two methods. E-P loops were reported to usually occur within the range of 1–200 kb (Hsieh et al. 2020). Distribution of interaction contacts and *P(s)* analysis showed that Trac-looping produced more short-range *cis* interactions (<20 kb), whereas OCEAN-C and Hi-C generated more long-range *cis* interactions (>20 kb), and in comparison, NicE-C generated relative even *cis* interactions in both short and long ranges (Supplemental Fig. S9B–D).

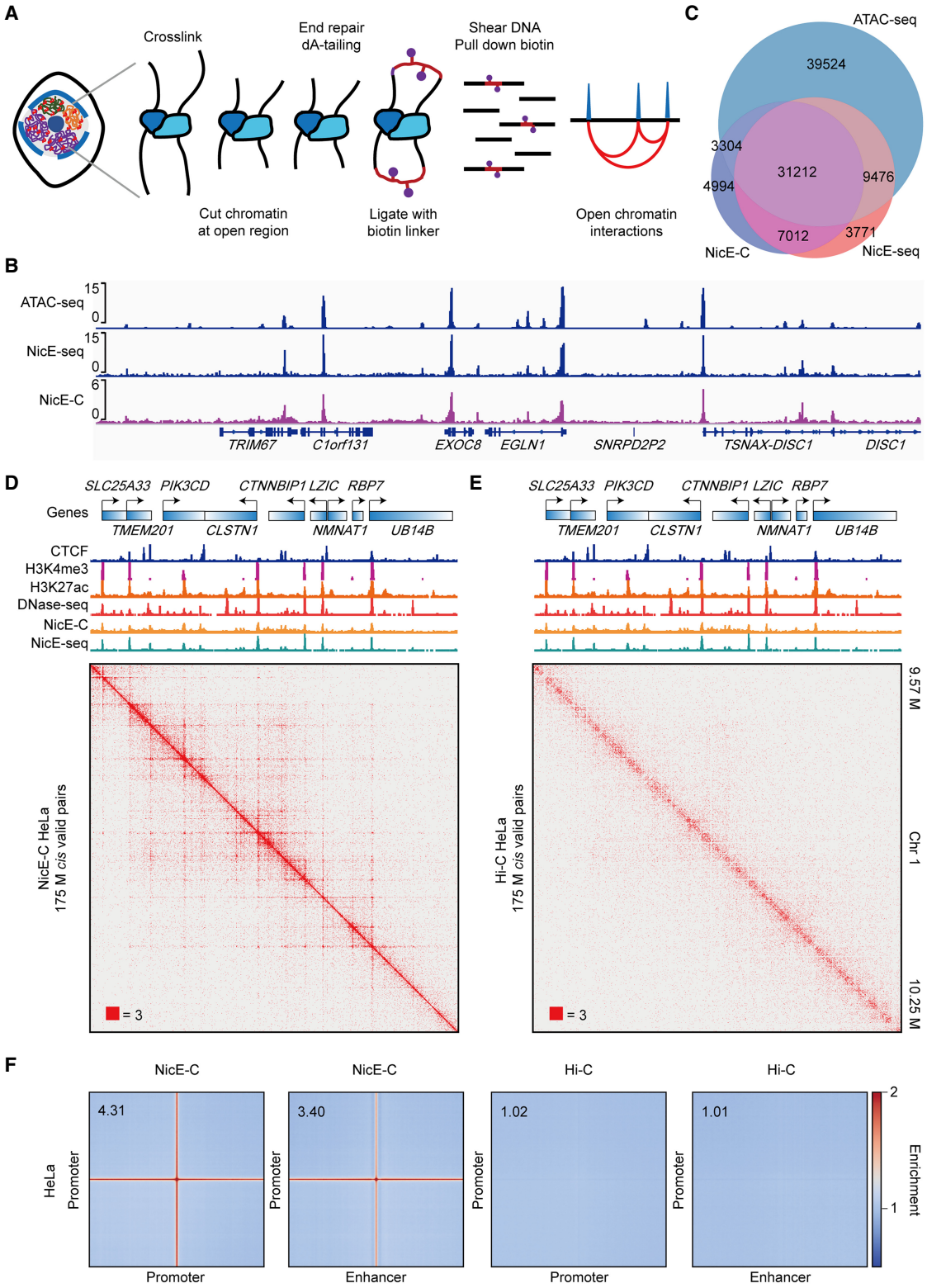

Figure 1. NicE-C discovers open chromatin–associated chromatin interactions. (*A*) Schematic of the NicE-C method. (*B*) A snapshot of chromatin accessibility detected by NicE-C, NicE-seq, and published ATAC-seq data for HeLa cells. (*C*) Venn diagram of open chromatin peaks identified by NicE-C, NicE-seq, and published ATAC-seq data. (*D*,*E*) HeLa NicE-C (*D*) and Hi-C (*E*) chromatin contact maps of an example region on Chromosome 1 at 1-kb resolution. Snapshots of 1D chromatin tracks (ChIP-seq of CTCF, H3K4me3 and H3K27ac, DNase-seq [for references, see Methods], open chromatin signal of NicE-C and NicE-seq) in this region are also shown. Numbers *below* the interaction maps correspond to the maximum signal in the matrix. (*F*) Genome-wide averaged pile-up matrices (plotted at 1-kb resolution, windows = 200 kb) showing promoter–promoter/promoter–enhancer interactions (P-P/E-P loops) and stripes detected by NicE-C (HeLa) and Hi-C (HeLa).

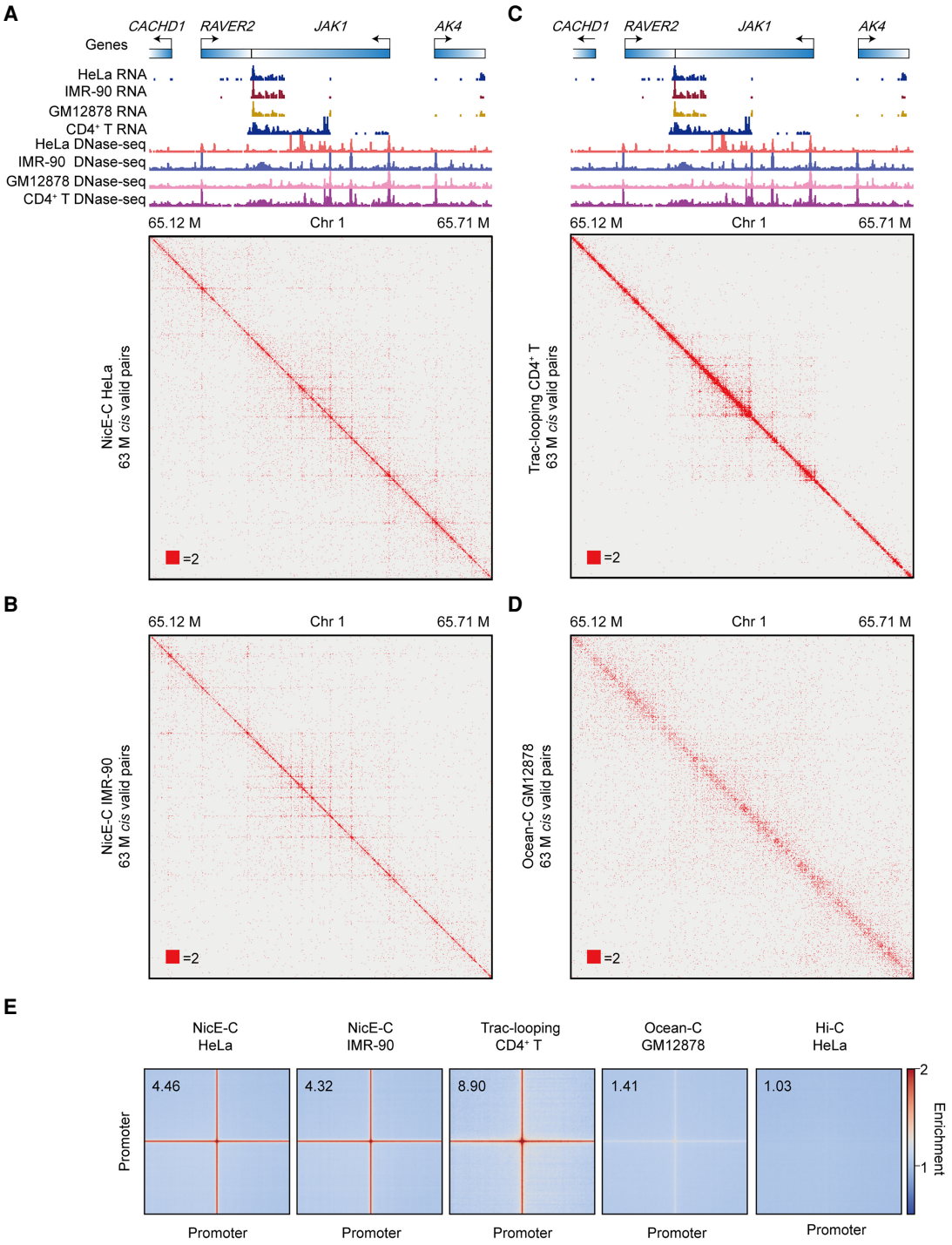

Figure 2. Open chromatin interactions captured by NicE-C, Trac-looping, and OCEAN-C. (*A–D*) HeLa cells NicE-C (*A*), IMR-90 cells NicE-C (*B*), CD4$^+$ T cells Trac-looping (*C*), and GM12878 cells OCEAN-C (*D*) chromatin contact maps of an example region (TPM value of *JAK* gene for these four cells are approximately 120) on Chromosome 1 at 1-kb resolution. Heatmaps were plotted with equal *cis* valid pairs. The RefSeq genes, RNA-seq, and DNase-seq signal of four different cell lines are also shown. (*E*) Genome-wide averaged pile-up matrices (plotted at 1-kb resolution, windows = 200 kb) showing P-P interactions and stripes detected by NicE-C (HeLa cells and IMR-90 cells), Trac-looping (CD4$^+$ T cells), OCEAN-C (GM12878 cells), and Hi-C (HeLa cells).

Considering that the NicE-C, Trac-looping, and OCEAN-C data were generated from different cells, we selected a genomic region for comparison wherein all of the cells displayed similar gene expression levels based on RNA-seq. The results showed that NicE-C and Trac-looping could provide informative open chromatin interactions at 1-kb resolution, whereas OCEAN-C provide very weak interactions, if any, with the same *cis* valid pairs (Fig. 2A–D). Genome-wide analyses showed that all three methods could enrich P-P loops and stripes compared to Hi-C, with NicE-C and Trac-looping showing much stronger enrichment over OCEAN-C (Fig. 2E).

To evaluate the sensitivity of related methods—Trac-looping typically starts with 100 M cells and OCEAN-C needs ~1 M cells (Lai et al. 2018; Li et al. 2018)—these large amounts of starting materials would limit the ability to detect the function of E-P loops in rare clinical samples. We then compared the NicE-C data generated with 1 M and 0.1 M cells to check whether NicE-C could capture E-P loops with reduced starting materials. Although the PCR duplication ratio was increased to ~77% for 0.1 M cells compared to ~43% for 1 M cells with a similar sequencing depth (Fig. 3A), the NicE-C data from 0.1 M cells still efficiently captured similar amount of open chromatin peaks and interactions compared to those from 1 M cells (Fig. 3B–E). These results suggested that NicE-C is a sensitive method to detect open chromatin interactions with about 0.1 M starting cells. These results collectively support NicE-C as a high-resolution, low-input, and informative open chromatin interaction capture method.

We further explored the application of NicE-C to detect changes in E-P loops between different cellular states. Specifically,

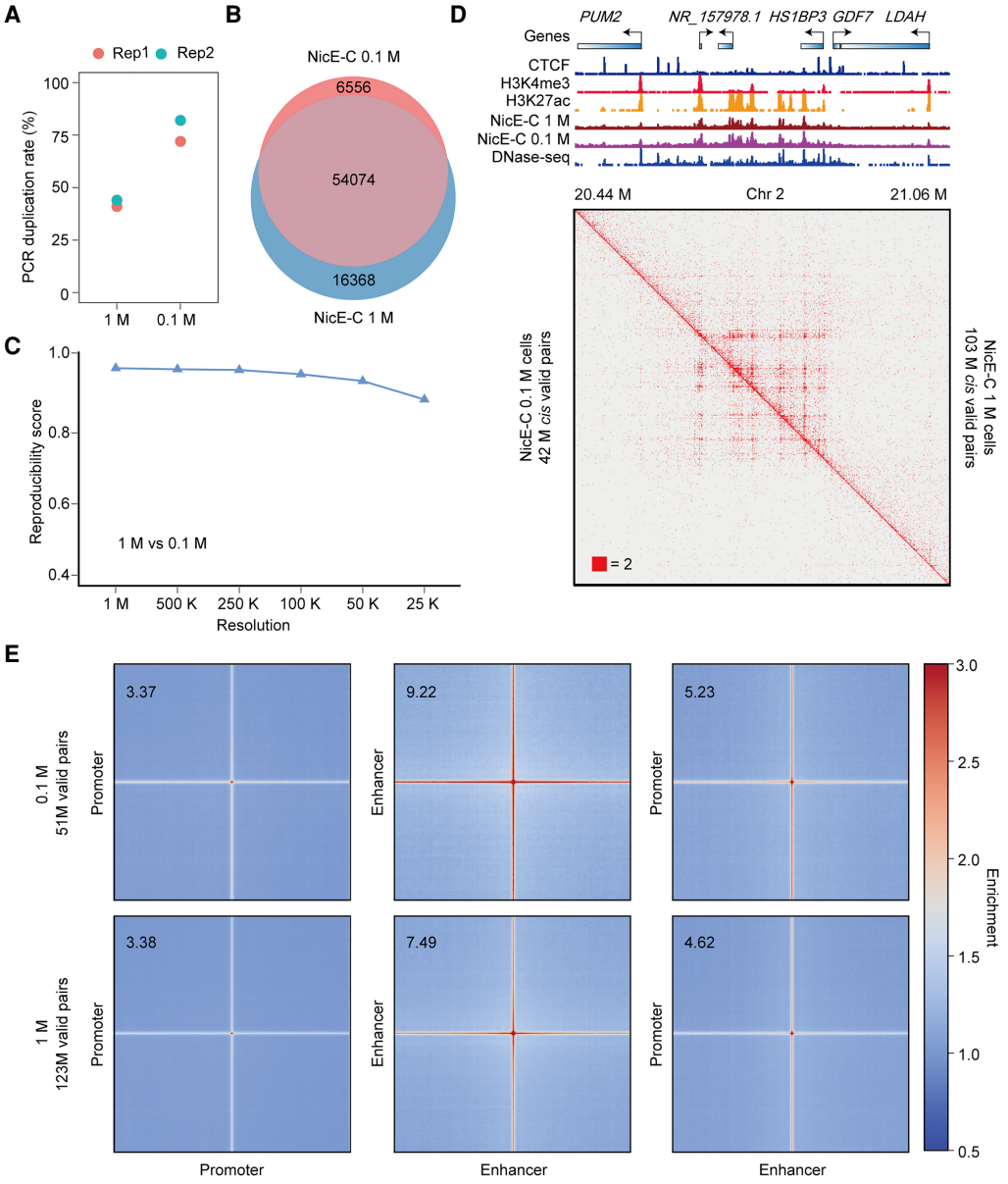

Figure 3. Comparison of NicE-C with 1 M and 0.1 M HeLa S3 cells. (*A*) PCR duplication rates of NicE-C (approximately 420 M reads) with 1 M and 0.1 M input cells. (*B*) Venn diagram of open chromatin peaks identified by NicE-C with 1 M and 0.1 M input cells. (*C*) Reproducibility analysis of 1 M cells and 0.1 M cells NicE-C data. Reproducibility scores were calculated by HiC-Rep at different resolutions. (*D*) NicE-C chromatin contact maps of an example region on Chromosome 2 at 1-kb resolution; the *top right* of the heatmap showed the NicE-C data with 1 M input cells, and the *bottom left* of the heatmap showed the NicE-C with 0.1 M input cells. Snapshots of 1D chromatin tracks (ChIP-seq of CTCF, H3K4me3, and H3K27ac, and open chromatin signals of NicE-C and DNase-seq) in this region are also shown. Numbers *below* the interaction maps correspond to maximum signal in the matrix. (*E*) Genome-wide averaged pile-up matrices of P-P, E-E, and E-P loops and stripes were plotted at 1-kb resolution (windows = 200 kb). The *top* plots showed NicE-C data with 0.1 M input cells, and the *bottom* plots showed NicE-C data with 1 M input cells.

we performed NicE-C and RNA-seq for HeLa S3 cells with or without TNF stimulation or on young versus old mouse kidney tissues. We found that 223 genes increased expression after TNF stimulation, whereas only 38 genes down-regulated. Compared to unchanged genes, the promoters of up-regulated genes showed increased enrichment of chromatin interactions with enhancers or other promoters in TNF-stimulated cells (Supplemental Fig. S10A,B). As one specific example, the "TNF alpha induced protein 3" (*TNFAIP3*) gene displayed a ~200-fold induction upon TNF stimulation according to our RNA-seq data (Fig. 4A). The NicE-C

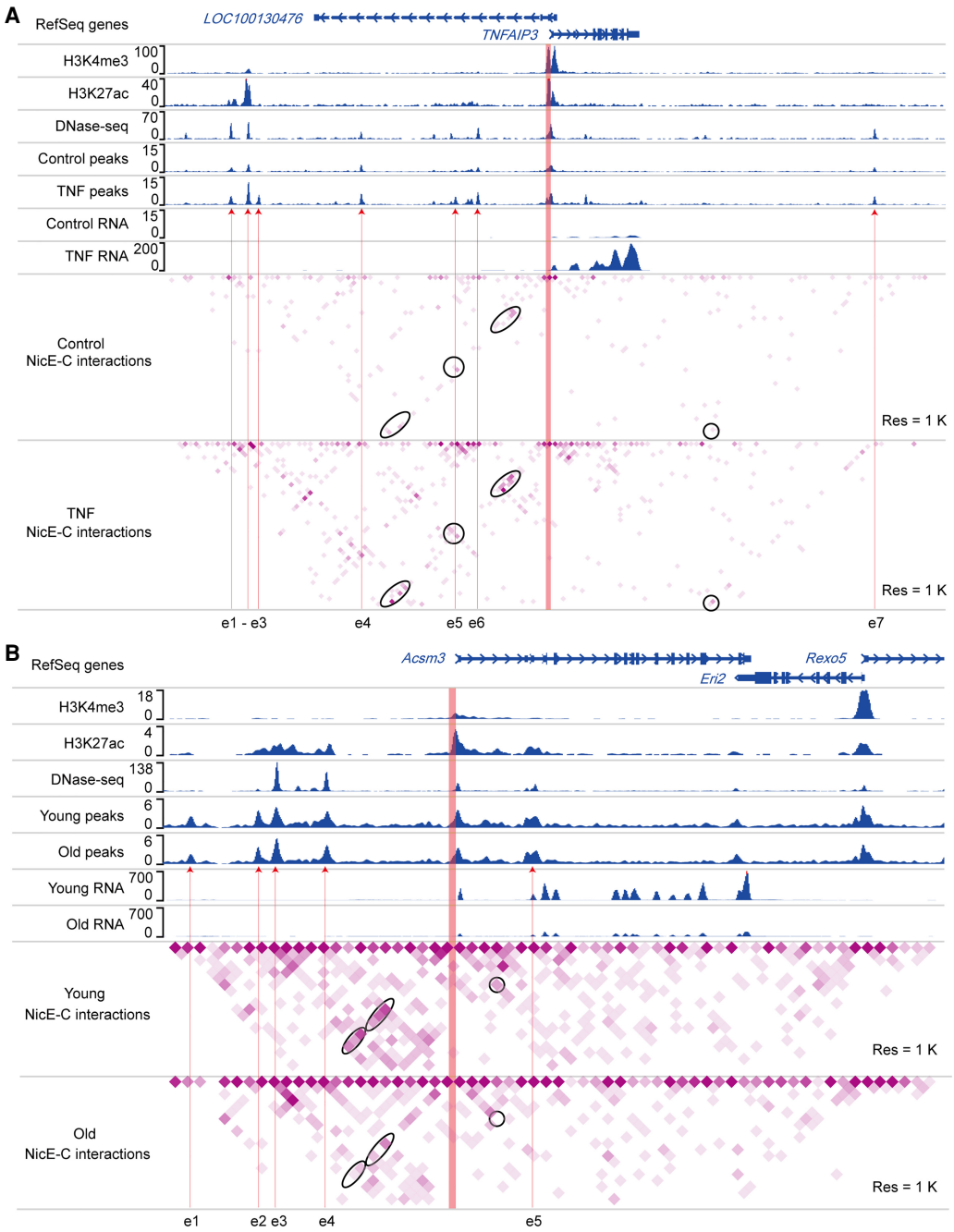

Figure 4. Dynamic enhancer–promoter interactions detected by NicE-C. (*A*) An example of TNF-stimulation-induced changes in E-P loops around the *TNFAIP3* locus, detected by NicE-C. Snapshots of 1D chromatin tracks (ChIP-seq of H3K4me3 and H3K27ac, and DNase-seq [for references, see Methods]; open chromatin signals of NicE-C, and RNA-seq) in the example region are also shown. Red arrows pointing to e1 to e6 show the putative enhancers based on ChIP-seq, DNase-seq, and our NicE-C peaks. The region in orange represents the gene promoter. Ovals indicate examples of increased interactions associated with indicated gene promoter in TNF-treated cells compared to control cells. (*B*) An example of E-P loops in old mouse kidney compared to those in young mouse kidney around the *Acsm3* locus (down-regulated gene in old mouse kidney), detected by NicE-C. Snapshots of 1D chromatin tracks (ChIP-seq of H3K4me3 and H3K27ac, DNase-seq, and open chromatin signals of NicE-C and RNA-seq) in this region are also shown. Red arrows pointing to e1 to e4 show the putative enhancers based on ChIP-seq, DNase-seq, and our NicE-C peaks. The region in orange represents the gene promoter. Ovals indicate examples of decreased interactions associated with indicated gene promoter in old kidney compared to young kidney.

data showed that the promoter of *TNFAIP3* formed multiple interactions with nearby enhancers, which were not detectable in untreated control cells (Fig. 4A). Relative to young mouse kidney tissues, we identified 310 up-regulated genes and 257 down-regulated genes in old kidney tissues, consistent with previous findings that kidney aging accompanied with increased immune infiltration, decreased mitochondrial function, and significantly up-regulated transporter genes on the apical side (Takemon et al. 2021). We found that the promoters of up- or down-regulated genes tend to interact with enhancers or other promoters with more or less frequency (Supplemental Fig. S10C–F). For example, the promoter of down-regulated gene acyl-CoA synthetase medium-chain family member 3 (*Acsm3*), which encoded a protein located to mitochondria, showed decreased interactions with nearby enhancers in old kidney compared to those in young kidney (Fig. 4B). The promoter of the up-regulated gene solute carrier family 7 (cationic amino acid transporter, y+ system), member 12 (*Slc7a12*), belonging to transporter genes on the apical side, formed more interactions with nearby enhancers in old kidney compared to those in young kidney (Supplemental Fig. S11). These results showed that NicE-C can detect dynamic E-P loops that are tightly linked to gene transcription changes.

Discussion

Enhancer–promoter communications play critical roles in transcription regulation (Rao et al. 2014; Bonev et al. 2017; Weintraub et al. 2017; Hua et al. 2018). However, current methods for detecting E-P interactions are not convenient or efficient, limiting their ability to study the function and dynamic of E-P interactions during biological processes or diseases. Here, we have established a high-resolution NicE-C method for *cis*-regulatory elements associated chromatin interactions capture, especially the interactions between enhancers and promoters, from 0.1 to 1 M cells at 1-kb resolution. We showed that NicE-C can detect E-P/P-P loops and stripes, and these interactions are tightly linked to gene transcription. NicE-C is an easy-to-operate method because the overall procedure of NicE-C is similar to that of Hi-C, with nicking enzyme–mediated open chromatin digestion replacing restriction enzyme in Hi-C. In addition, NicE-C is also a time-saving method that can be finished in 2 d, compared to 3 d for Ocean-C and 4 d for Trac-looping.

Dynamic chromatin interactions of *cis*-regulatory elements in the nucleus pose a challenge for studying diseases because noncoding risk variants often locate far from their regulated genes. Previous studies based on promoter Capture Hi-C showed that promoter-associated chromatin interactions could link noncoding genome-wide association studies (GWAS) variants with putative target genes and the promoter-interacting regions enriched for expression quantitative trait loci (eQTLs) (Javierre et al. 2016), revealing the unique value of *cis*-regulatory elements interaction in elucidating disease etiology. Clinical samples from patients are often limited, thus the genome-wide promoter Capture Hi-C (~20 M cells) and Trac-looping (~100 M cells) are not suitable for detecting the dynamics of E-P interactions associated with diseases. Ocean-C could start with approximately 1 M cells, but the resolution of *cis*-regulatory elements associated interactions detected by Ocean-C is relatively lower compared to other methods. We have showed that NicE-C can be used to informatively track dynamic changes of E-P/P-P loops across different cellular conditions with limited starting materials. We thus believe that NicE-C is more appropriate for studying *cis*-regulatory elements associated interactions in disease.

We showed that NicE-C is an easy-to-implement, time-saving, and efficient method for profiling E-P loops at high resolution. Although NicE-C requires the least starting materials among published open chromatin–associated chromatin interaction capture methods, it is still not compatible with single-cell profiling. Further optimization is still needed to push the NicE-C method in delineating open chromatin interactions and precision E-P communications to single-cell levels.

Methods

Cells and animals

HeLa cells, HeLa-S3 cells, and IMR-90 cells were grown in DMEM medium containing 10% fetal bovine serum (FBS) at 37°C and 5% CO_2. The cells were cultured to 70%–80% confluence and then used for further experiments. C57BL/6 mice were originally purchased from Vital River Laboratories in Beijing, China. The mice were housed in the Animal Center of the University of Science and Technology of China and were cultured under a 12-h light/dark cycle (lights off at 7 p.m.) at 23°C ± 2°C. All animal experiments were performed in accordance with the guidelines of and approved by the University of Science and Technology of China (USTC) Animal Resources Center and University Animal Care and Use Committee (permit number: USTCACUC1801015).

Cell treatment and cross-link

For cross-linking, cultured cells were collected by trypsin and then fixed at room temperature for 10 min with 1% formaldehyde (Sigma-Aldrich F8775-500ML). After cross-linking, 2.5 M Glycine (Sigma-Aldrich G8898-1KG) was added to the final 125 mM and incubated at room temperature for 10 min to quench the reaction. Fixed cells were pelleted and washed twice with ice-cold 1× PBS. After removing the supernatant, the fixed cells were stored at –80°C until used. TNF (Sino biological 10602-HNAE) was dissolved in water to a final concentration of 20 ng/μL. Cultured HeLa-S3 cells were washed once with 1× PBS, and fresh DMEM media supplemented with final 10 ng/mL TNF or water were added. Cells were then incubated for 60 min and subjected to NicE-C or RNA-seq.

Dissociation of cells from mouse kidneys

Mouse kidneys were dissected and minced to small pieces by surgical scissors in ice-cold 1× PBS and were transferred to the top of a 40 μm cell strainer (Sorfa 251100) and pelleted at 500*g* for 3 min at 4°C. The cells were fixed at room temperature for 10 min with 1% formaldehyde. After cross-linking, final 125 mM Glycine was added and incubated at room temperature for 10 min to quench the reaction. Fixed cells were pelleted and washed twice with ice-cold 1× PBS. After removing the supernatant, the fixed cells were stored at –80°C until used.

NicE-seq library preparation

NicE-seq was performed following the published protocol with slight modifications (Ponnaluri et al. 2017; Chin et al. 2020). In brief, 1 million fixed cells were resuspended in 1 mL of cytosolic buffer (15 mM Tris-HCl pH 7.5, 5 mM $MgCl_2$, 60 mM KCl, 0.5 mM DTT, 15 mM NaCl, 300 mM sucrose, and 1% NP-40), incubated on ice for 10 min, and pelleted at 800*g* for 3 min at 4°C. The pellet was resuspended in the following reaction: 0.5 μL of Nt.CviPII (NEB R0626S), 2 μL of DNA Polymerase I (NEB M0209L), 3 μL of 1 mM dTTP, dGTP, biotin-14-dATP (Jena Bioscience NU-835-

BIO14-S) and 1.5 µL of 1 mM biotin-14-dCTP (Jena Bioscience NU-956-BIO14-S), 5-methyl-dCTP (NEB, N0356S), 40 µL 50% PEG8000 in 200 µL 1× NEBuffer2. The nuclei were incubated at 37°C for 25 min for open chromatin labeling with interval shaking (950 rpm, 15 sec every 2 min). The nuclei were pelleted at 800*g* for 3 min, then resuspended in 300 µL reverse cross-linking buffer (20 mM Tris pH 8.0, 20 mM NaCl, 0.1% Triton X-100, 15 mM DTT, 1 mM EDTA) containing 10 µL Proteinase K (Thermo Fisher Scientific EO0492) and incubated overnight at 65°C. DNA were purified with HiPure Gel Pure DNA Mini Kit (Magen D2111-03) and then sonicated to 200- to 400-bp fragments. The DNA fragments were then mixed with 30 µL of washed Dynabeads M-280 (Thermo Fisher Scientific 11205D) and incubated at room temperature for 30 min for open chromatin selecting with slow rotation. End repair, dATP tailing, adapter ligation, and PCR amplification were performed with selected DNA sequentially. The PCR products were size selected with VAHTS DNA Clean Beads (Vazyme N411-01), and the libraries were sequenced via Illumina NovaSeq platforms.

Bridge linker preparation for NicE-C

For NicE-C bridge linker ligation, three biotinylated bridge linkers:

Bridge linker B1: 5′-[5Phos]TGCGGA/iBIOdT/CCGCAT-3′,
Bridge linker B2: 5′-[5Phos]ACCGGA/iBIOdT/CCGGTT,
Bridge linker H: 5′-[5Phos]TGCAAGCT/iBIOdT/GCAT,

with the 3′ nucleotide T overhanging on both strands after annealing were used (NicE-C libraries prepared with Bridge linker B1 and B2 can be digested with BamHI to estimate the portion of biotinylated junctions, NicE-C libraries prepared with Bridge linker H can be digested with HindIII to estimate the proportion of biotinylated junctions). Bridge linkers were dissolved in 1× NEBuffer2 to a concentration of 100 µM and annealed on the PCR machine as follows: for 2 min at 95°C, then hold for 30 sec at each cycle with a drop of 0.5°C/cycles for 140 cycles to final 25°C. The annealed bridge linkers were stored at −20°C.

NicE-C library preparation

Chromatin digestion

One million or 0.1 million fixed cells were resuspended in 1 mL of cytosolic buffer (15 mM Tris-HCl pH 7.5, 5 mM $MgCl_2$, 60 mM KCl, 0.5 mM DTT, 15 mM NaCl, 300 mM sucrose, and 1% NP-40), incubated on ice for 10 min and pelleted at 800*g* for 3 min at 4°C. The pellet was resuspended in the following reaction: 0.5 µL of Nt.CviPII (NEB R0626S), 2 µL of DNA Polymerase I (NEB M0209L), 3 µL of 1 mM dTTP, dGTP and dATP, 1.5 µL of 1 mM dCTP and 5-methyl-dCTP (NEB N0356S), 40 µL 50% PEG8000 in 200 µL 1× NEBuffer2. The nuclei were incubated for 25 min at 37°C for chromatin digestion at open region with interval shaking (950 rpm, 15 sec every 2 min). Five hundred millimolar EDTA was added to the final 30 mM and incubated for 20 min at 65°C to stop the reaction, then the nuclei were pelleted at 800*g* for 2 min.

Troubleshooting

The chromatin digestion efficiency is important for NicE-C. To determine the efficacy of chromatin digestion at open chromatin regions, take 20 µL of digested cells from the previous step. Add 170 µL reverse cross-linking buffer and 10 µL Proteinase K, incubate for 30 to 60 min at 65°C. Then purify DNA with HiPure Gel DNA Mini Kit and check the quality of chromatin digestion by running the purified DNA on a 1% agarose gel. The sample is properly digested if one sees a large smear of DNA fragments between ~4 kb to 12 kb (see Supplemental Fig. S1A, 20 min). We recommend characterizing NicE-C chromatin digestion efficiency when performing the NicE-C with a new cell type or new tissue sample. In the event of overdigestion of chromatin, we recommend optimizing the amount of Nt.CviPII and DNA Polymerase I used, or the digestion time.

Chromatin end repair and dA tailing

After chromatin digestion and reaction stop, washing twice with NicE-C wash buffer (2 mM $MgCl_2$, 1× BSA, 2.5% PEG8000, 0.05% SDS, 0.2% Triton X-100), the nuclei were resuspended in 400 µL 1 × T4 ligase buffer containing 20 µL of 10% Triton X-100, 20 µL of 50% PEG8000, 10 µL of 10 mM dNTPs, 10 µL of T4 Polynucleotide Kinase (NEB, M0201S), 8 µL of T4 DNA Polymerase (NEB M0203S), 2 µL of Klenow (NEB M0210S). Then, the nuclei were incubated for 60 min at 37°C for end repair with interval shaking (950 rpm, 15 sec every 2 min). Five hundred millimolar EDTA was added to the final 30 mM and incubated for 20 min at 65°C to stop the reaction. After washing twice with NicE-C wash buffer, the nuclei were resuspended in 400 µL 1× NEBuffer2 containing 20 µL of 10% Triton X-100, 20 µL of 50% PEG8000, 10 µL of 10 mM dATP, 10 µL of Klenow (exo-) (NEB M0212S). Then, the nuclei were incubated for 60 min at 37°C for dA tailing with interval shaking (950 rpm, 15 sec every 2 min). Five hundred millimolar EDTA was added to the final 30 mM and incubated for 20 min at 65°C to stop the reaction.

Chromatin ligation with biotin-labeled bridge linker

After dA tailing and reaction stop, washing twice with NicE-C wash buffer, the nuclei were resuspended in 600 µL 1× T4 DNA ligase buffer containing 30 µL of 10% Triton X-100, 30 µL of 50% PEG8000, 20 µL of 50 µM bridge linker, 4 µL of T4 DNA ligase (NEB M0202S). Then, the nuclei were incubated for 4 h at 23°C for proximity ligation with interval shaking (1100 rpm, 15 sec every 2 min).

Sequencing library generation

For starting with 1 M or more cells: after ligation, reverse cross-linking, DNA purification, DNA fragmentation were performed sequentially. The DNA fragments were then mixed with 30 µL of washed Dynabeads M-280 and incubated for 30 min at room temperature for biotin-labeled fragments selecting with slow rotation. End repair, dATP tailing, adapter ligation, and PCR amplification were performed with selected DNA sequentially. The PCR products were size selected with VAHTS DNA Clean Beads (Vazyme N411-01), and the libraries were sequenced via Illumina NovaSeq platforms.

For starting with 0.1 M cells: after ligation and reverse cross-linking, sonication was used to shear the DNA without DNA purification to reduce the loss of DNA. After sonication, the DNA fragments in reverse cross-linking buffer were then mixed with 10 µL of washed Dynabeads M-280 and incubated for 30 min at room temperature for biotin-labeled fragments selecting with slow rotation. End repair, dATP tailing, adapter ligation, and PCR amplification were performed with selected DNA sequentially. The PCR products were size selected with VAHTS DNA Clean Beads (Vazyme N411-01), and the libraries were sequenced via Illumina NovaSeq platforms.

In situ Hi-C library preparation

In situ Hi-C was performed following the published protocol with slight modifications (Rao et al. 2014). In brief, 1 million fixed cells were resuspended in 1 mL of ice-cold Hi-C lysis buffer (10 mM Tris,

pH 8.0, 10 mM NaCl, 0.2% Igepal CA-630 and 1× complete protease inhibitors) and incubated on ice for 15 min. The nuclei were pelleted and resuspended in 50 μL of 0.5% (w/v) SDS (Thermo Fisher Scientific 24730020), incubated for 10 min at 62°C. Then, 25 μL 10% (v/v) Triton X-100 (Sigma-Aldrich X100-100ML) and 145 μL of water were added to the tube and incubated for 10 min at 37°C with shaking to quench SDS. The volume was brought to 400 μL with final 1× NEBuffer2 containing 200 units of MboI (NEB R0147M) and incubated overnight at 37°C for chromatin digestion with shaking at 900 rpm. The next day, it was incubated for 20 min at 62°C to inactivate MboI. Then, biotin-14-dATP (Jena Bioscience NU-835-BIO14-S), dCTP, dTTP, dGTP and Klenow (NEB M0210S) were added for biotin fill in by incubating for 90 min at 37°C. Then 10× T4 DNA ligase buffer, 100× BSA, 10% Triton X-100 and T4 DNA ligase (NEB M0202S) were added for proximity ligation by incubating for 4 h at 25°C with slow rotation. After ligation, reverse cross-linking, DNA purification, DNA fragmentation were performed sequentially. The DNA fragments were then mixed with 30 μL of washed Dynabeads M-280 and incubated for 30 min at room temperature for biotin-labeled fragments selecting with slow rotation. End repair, dATP tailing, adapter ligation, and PCR amplification were performed with selected DNA sequentially. The PCR products were size selected with VAHTS DNA Clean Beads (Vazyme N411-01), and the libraries were sequenced via Illumina NovaSeq platforms.

RNA-seq

One million TNF-treated, control HeLa-S3 cells, or dissociated mouse kidney cells were collected, respectively, and resuspended in 1 mL of TRIzol (Invitrogen 15596018) according to the manufacturer's instructions. RNA purification and sequencing library construction were performed by Berry Genomics, then the libraries were sequenced via Illumina NovaSeq platforms.

NicE-C, NicE-seq, and ATAC-seq peak identification and correlation analysis

We mapped NicE-C, NicE-seq reads, and published ATAC-seq data (Cho et al. 2018) to hg19 or mm9 genome by Bowtie 2 (Langmead and Salzberg 2012). We also mapped the reads of some samples to hg38 or mm10 and found that their genome-wide profiles are highly similar to that mapped to hg19 or mm9. Thus, we believe that the use of hg19 or mm9 in this study would not affect the conclusion. MACS2 (Zhang et al. 2008) was used to call peaks. Overlap of Open chromatin peaks in ATAC-seq, NicE-seq, and NicE-C were identified using BEDTools (Quinlan and Hall 2010). Sample correlations were analyzed based on the output of multiBamSummary function of deepTools (Ramírez et al. 2014), and the Spearman method was used to compute correlation coefficients. The intersect function of BEDTools was used to count the number of reads mapped to each peak. The count matrix was normalized by reads per million (RPM) mapped reads. Pearson correlation coefficients between biological replicates of mouse kidneys NicE-C were calculated based on the $\log_{10}$ RPM matrix.

ChIP-seq analysis

Public H3K27ac and H3K4me3 ChIP-seq data sets of HeLa cell and IMR-90 cell were downloaded from the NCBI Gene Expression Omnibus (GEO; https://www.ncbi.nlm.nih.gov/geo/; accession numbers GSM1670864, GSM1670868, GSM1846779, GSM1846782, GSM2774992, GSM2774993, GSM2774994, GSM2774995, GSM1055816) and mapped to hg19 genome by Bowtie 2. We also mapped the reads of some samples to hg38 and found that their genome-wide profiles are highly similar to that mapped to hg19. Thus, we believe that the use of hg19 in this study would not affect the conclusion. Peaks were called by MACS2 peak analysis function. Regions with H3K27ac enrichment but without H3K4me3 enrichment were identified as enhancer regions.

RNA-seq analysis

The FASTQ files of RNA-seq were mapped to the human genome (hg19) or mouse genome (mm9) with HISAT2 (Pertea et al. 2016). We also mapped the reads of some samples to hg38 or mm10 and found that their genome-wide profiles are highly similar to that mapped to hg19 or mm9. Thus, we believe that the use of hg19 or mm9 in this study would not affect the conclusion. Counts per gene were determined with HTSeq (Anders et al. 2015). Genes with significantly (fold change > 2, P-adj < 0.05) increased or decreased expression levels after TNF treatment or during mice aging process were identified with DESeq2 (Love et al. 2014).

Mapping, pairing, and browsing of NicE-C and Hi-C data

Valid NicE-C and Hi-C contact read pairs were obtained from HiC-Pro (Servant et al. 2015). Briefly, paired-end reads were mapped to hg19 or mm9 reference genome separately by Bowtie 2 (Global option: --very-sensitive -L 30 --score-min L,-0.6,-0.2 --end-to-end --reorder, local option: --very-sensitive -L 20 --score-min L,-0.6,-0.2 --end-to-end --reorder). We also mapped the reads of some samples to hg38 or mm10 and found that their genome-wide profiles are highly similar to that mapped to hg19 or mm9. Thus, we believe that the use of hg19 or mm9 in this study would not affect the conclusion. To rescue the chimeric fragments spanning the ligation junction, the ligation site was detected and the 5′ end fraction of the reads was aligned back to the reference genome. Pairs with multiple hits, low MAPQ, singleton, dangling end, self-circle, and PCR duplicates were removed. Output files containing all valid pairs were used in downstream analyses. The reproducibility of NicE-C and Hi-C valid pairs were evaluated by Hi-Rep (Yang et al. 2017). For the downstream analysis, valid pairs obtained from biological replicates were pooled because the biological replicates showed high reproducibility. The valid pairs were then converted to HIC files using hicpro2juicebox.sh, provided by HiC-Pro for visualization with Juicebox (Durand et al. 2016) or WashU Epigenome Browser (Li et al. 2019). We selected an equal number of *cis* valid pairs to the generated HIC file and COOL file when comparing the chromatin contact heatmaps or pile-up analysis of E-P/P-P interactions between different methods or samples in this study.

The normalization methods used for 3D data can be divided into explicit and implicit approaches according to the principle. Implicit approaches assume that each bin has the same sequencing coverage. NicE-C combined NicE-seq and in situ Hi-C to efficiently capture chromatin interactions associated with open chromatin regions which was more similar to PLAC-seq (Fang et al. 2016) and HiChIP (Mumbach et al. 2016), which both capture chromatin interactions anchored at genomic regions compared to Hi-C. The matrix-balancing-based normalization methods (ICE, VC, or KR) used for Hi-C data assumed that all genomic regions have equal visibility and is invalid for NicE-C and PLAC-seq/HiChIP data because not all the genomic regions are opened or bound by the target proteins.

Alternatively, explicit approaches assume that the systematic biases, such as fragment length, GC content, and sequence mappability, are known and accounted for in the statistical model. HiCNorm and MAPS are explicit methods used for PLAC-seq and HiChIP data normalization, which generated a local genomic

features file based on a specific restriction endonuclease site and used in data normalization. However, currently, we used Nt.CviPII and DNA Polymerase I for chromatin fragmentation at open chromatin regions in NicE-C, and we found that the chromatin ends generated in NicE-C were not limited to CCD. Owing to the NicE-C procedure and the unclear fragmentated chromatin ends, the HiCNorm and MAPS were also not suitable for NicE-C data normalization.

A/B compartments, TADs, and chromatin loops

For comparing the A/B compartments, TADs, and chromatin loops in HeLa cells identified by NicE-C and Hi-C, we converted HIC files to HDF5 format as COOL files by cooler (Abdennur and Mirny 2020). Saddle plots of A/B compartments were generated by the compute-saddle tool in cooltools (https://github.com/mirnylab/cooltools). The upper-left and bottom-right of the saddle plot represent the contact frequency between B-B and A-A compartments, the upper-right and bottom left of the saddle plot represent the contact frequency between A and B compartments. Published HeLa TADs and chromatin loops (Rao et al. 2014) were used for pile-up analysis with COOL files generated from NicE-C and Hi-C data. The rescaled pile-up analysis and plot of TADs (1-kb bins) and the pile-up analysis and plot of chromatin loops (1-kb bins) were generated by coolpup.py (Flyamer et al. 2020). High confidence interactions in HeLa NicE-C data were identified using cLoops (Cao et al. 2020) with parameters -eps 1000,2000 -minPts 10 -w -j -cut 2000 -s -max_cut -plot.

Pile-up analysis of open chromatin interactions

Genome-wide open chromatin interactions between promoter–promoter (P-P), promoter–enhancer (P-E), and enhancer–enhancer (E-E) were assessed by pile-up analysis such as the pile-up analysis of chromatin loops described above. The COOL files of Hi-C, NicE-C, and published Trac-looping (Lai et al. 2018) or OCEAN-C (Li et al. 2018) data were generated by cooler. The cell- and tissue-specific enhancers were identified with published H3K4me3 and H3K27ac ChIP-seq data. The pile-up analysis of P-P, P-E, and E-E interactions were performed with coolpup.py.

Chromatin random conversion ratio count

NicE-C, Ocean-C, and Trac-looping valid pairs were used for counting chromatin random conversion ratio. The number of hybrid valid pairs with ends from Nuclear DNA (n) and Mitochondrion DNA (m) was denoted by N_{nm}. Total valid pairs number was denoted by N_{total}. We calculated the ratio of chromatin random conversion by N_{nm}/N_{total}.

TAD boundary analysis and genome-wide distance versus counts plot

For TAD boundary analysis for HeLa cells, we converted the HIC file of Hi-C data to HDF5 format as a COOL file by cooler (Abdennur and Mirny 2020). Then, we used the hicFindTADs function in HiCExplorer (Ramírez et al. 2018) for TAD boundary identification. We only used *cis* chromatin contacts for genome-wide distance versus counts plot. The COOL files at 1-kb resolution were generated by cooler. Then, the genomic distance versus chromatin counts plots were plotted by hicPlotDistVsCounts function in HiCExplorer (Ramírez et al. 2018) with the COOL files.

ENCODE and GEO data

ENCODE ChIP-seq and DNase-seq tracks displayed with chromatin contact heatmaps were loaded in Juicebox under the following accession numbers: ENCFF00YCP (IMR-90, CTCF ChIP-seq), ENCFF001LKR (mouse kidney, male, CTCF ChIP-seq), ENCFF000STL (IMR-90, DNase-seq), ENCFF247YYB (HeLa S3, DNase-seq), ENCFF001PNU (mouse kidney, male, DNase-seq), ENCFF000SLH (GM12878, DNase-seq), and ENCFF000SEP ($CD4^+$ T, human, DNase-seq). Other ChIP-seq, ATAC-seq, and RNA-seq tracks displayed with chromatin contact heatmaps were downloaded from the NCBI Gene Expression Omnibus (GEO; https://www.ncbi.nlm.nih.gov/geo/) under the following accession numbers: GSM4112813 (HeLa, CTCF ChIP-seq), GSM4112814 (HeLa, CTCF ChIP-seq), GSM2830381 (HeLa, ATAC-seq), GSM2830382 (HeLa, ATAC-seq), GSM5014656 (IMR-90, RNA-seq), GSM5014657 (IMR-90, RNA-seq), GSM3965459 (GM12878, RNA-seq), GSM3965460 (GM12878, RNA-seq), GSM2326184 ($CD4^+$ T, human, RNA-seq), and GSM2326185 ($CD4^+$ T, human, RNA-seq).

Data access

All raw and processed sequencing data generated in this study have been submitted to the NCBI Gene Expression Omnibus (GEO; https://www.ncbi.nlm.nih.gov/geo/) under accession number GSE176066.

Competing interest statement

The authors declare no competing interests.

Acknowledgments

This work was supported by the National Key Scientific Program of China (2016YFA0100502), the research project of the Joint Laboratory of University of Science and Technology of China and Anhui Mental Health Center (2019LH03), the Fundamental Research Funds for the Central Universities (WK2070210004), and China Postdoctoral Science Foundation (2021M703091).

Author contributions: Z.L., R.Z., T.H., and X.S. developed the method. Z.L., R.Z., and T.H. performed experiments. Z.L. and R.Z. analyzed the data. Z.L., R.Z., T.H., Y.Z., and X.S. wrote the manuscript. All authors discussed the results and edited the manuscript.

References

Abdennur N, Mirny LA. 2020. Cooler: scalable storage for Hi-C data and other genomically labeled arrays. *Bioinformatics* **36:** 311–316. doi:10.1093/bioinformatics/btz540

Anders S, Pyl PT, Huber W. 2015. HTSeq—a Python framework to work with high-throughput sequencing data. *Bioinformatics* **31:** 166–169. doi:10.1093/bioinformatics/btu638

Banigan EJ, van den Berg AA, Brandão HB, Marko JF, Mirny LA. 2020. Chromosome organization by one-sided and two-sided loop extrusion. *eLife* **9:** e53558. doi:10.7554/eLife.53558

Bonev B, Mendelson Cohen N, Szabo Q, Fritsch L, Papadopoulos GL, Lubling Y, Xu X, Lv X, Hugnot JP, Tanay A, et al. 2017. Multiscale 3D genome rewiring during mouse neural development. *Cell* **171:** 557–572.e524. doi:10.1016/j.cell.2017.09.043

Buenrostro JD, Giresi PG, Zaba LC, Chang HY, Greenleaf WJ. 2013. Transposition of native chromatin for fast and sensitive epigenomic profiling of open chromatin, DNA-binding proteins and nucleosome position. *Nat Methods* **10:** 1213–1218. doi:10.1038/nmeth.2688

Cao Y, Chen Z, Chen X, Ai D, Chen G, McDermott J, Huang Y, Guo X, Han JJ. 2020. Accurate loop calling for 3D genomic data with cLoops. *Bioinformatics* **36:** 666–675. doi:10.1093/bioinformatics/btz651

Chin HG, Sun Z, Vishnu US, Hao P, Cejas P, Spracklin G, Esteve PO, Xu SY, Long HW, Pradhan S. 2020. Universal NicE-seq for high-resolution accessible chromatin profiling for formaldehyde-fixed and FFPE tissues. *Clin Epigenetics* **12:** 143. doi:10.1186/s13148-020-00921-6

Cho SW, Xu J, Sun R, Mumbach MR, Carter AC, Chen YG, Yost KE, Kim J, He J, Nevins SA, et al. 2018. Promoter of lncRNA gene *PVT1* is a tumor-

suppressor DNA boundary element. *Cell* **173:** 1398–1412 e1322. doi:10.1016/j.cell.2018.03.068
Durand NC, Robinson JT, Shamim MS, Machol I, Mesirov JP, Lander ES, Aiden EL. 2016. Juicebox provides a visualization system for Hi-C contact maps with unlimited zoom. *Cell Syst* **3:** 99–101. doi:10.1016/j.cels.2015.07.012
Fang R, Yu M, Li G, Chee S, Liu T, Schmitt AD, Ren B. 2016. Mapping of long-range chromatin interactions by proximity ligation-assisted ChIP-seq. *Cell Res* **26:** 1345–1348. doi:10.1038/cr.2016.137
Flyamer IM, Illingworth RS, Bickmore WA. 2020. *Coolpup.py:* versatile pile-up analysis of Hi-C data. *Bioinformatics* **36:** 2980–2985. doi:10.1093/bioinformatics/btaa073
Fudenberg G, Imakaev M, Lu C, Goloborodko A, Abdennur N, Mirny Leonid A. 2016. Formation of chromosomal domains by loop extrusion. *Cell Rep* **15:** 2038–2049. doi:10.1016/j.celrep.2016.04.085
Giresi PG, Lieb JD. 2009. Isolation of active regulatory elements from eukaryotic chromatin using FAIRE (formaldehyde assisted isolation of regulatory elements). *Methods* **48:** 233–239. doi:10.1016/j.ymeth.2009.03.003
Hsieh TS, Cattoglio C, Slobodyanyuk E, Hansen AS, Rando OJ, Tjian R, Darzacq X. 2020. Resolving the 3D landscape of transcription-linked mammalian chromatin folding. *Mol Cell* **78:** 539–553 e538. doi:10.1016/j.molcel.2020.03.002
Hua JT, Ahmed M, Guo H, Zhang Y, Chen S, Soares F, Lu J, Zhou S, Wang M, Li H, et al. 2018. Risk SNP-mediated promoter-enhancer switching drives prostate cancer through lncRNA *PCAT19*. *Cell* **174:** 564–575.e518. doi:10.1016/j.cell.2018.06.014
Isoda T, Moore AJ, He Z, Chandra V, Aida M, Denholtz M, Piet van Hamburg J, Fisch KM, Chang AN, Fahl SP, et al. 2017. Non-coding transcription instructs chromatin folding and compartmentalization to dictate enhancer-promoter communication and T cell fate. *Cell* **171:** 103–119 e118. doi:10.1016/j.cell.2017.09.001
Javierre BM, Burren OS, Wilder SP, Kreuzhuber R, Hill SM, Sewitz S, Cairns J, Wingett SW, Varnai C, Thiecke MJ, et al. 2016. Lineage-specific genome architecture links enhancers and non-coding disease variants to target gene promoters. *Cell* **167:** 1369–1384.e1319. doi:10.1016/j.cell.2016.09.037
Krietenstein N, Abraham S, Venev SV, Abdennur N, Gibcus J, Hsieh THS, Parsi KM, Yang L, Maehr R, Mirny LA, et al. 2020. Ultrastructural details of mammalian chromosome architecture. *Mol Cell* **78:** 554–565.e7. doi:10.1016/j.molcel.2020.03.003
Lai B, Tang Q, Jin W, Hu G, Wangsa D, Cui K, Stanton BZ, Ren G, Ding Y, Zhao M, et al. 2018. Trac-looping measures genome structure and chromatin accessibility. *Nat Methods* **15:** 741–747. doi:10.1038/s41592-018-0107-y
Langmead B, Salzberg SL. 2012. Fast gapped-read alignment with Bowtie 2. *Nat Methods* **9:** 357–359. doi:10.1038/nmeth.1923
Li T, Jia L, Cao Y, Chen Q, Li C. 2018. OCEAN-C: mapping hubs of open chromatin interactions across the genome reveals gene regulatory networks. *Genome Biol* **19:** 54. doi:10.1186/s13059-018-1430-4
Li D, Hsu S, Purushotham D, Sears RL, Wang T. 2019. WashU Epigenome Browser update 2019. *Nucleic Acids Res* **47:** W158–W165. doi:10.1093/nar/gkz348
Lieberman-Aiden E, Van Berkum NL, Williams L, Imakaev M, Ragoczy T, Telling A, Amit I, Lajoie BR, Sabo PJ, Dorschner MO. 2009. Comprehensive mapping of long-range interactions reveals folding principles of the human genome. *Science* **326:** 289–293. doi:10.1126/science.1181369
Love MI, Huber W, Anders S. 2014. Moderated estimation of fold change and dispersion for RNA-seq data with DESeq2. *Genome Biol* **15:** 550. doi:10.1186/s13059-014-0550-8
Mifsud B, Tavares-Cadete F, Young AN, Sugar R, Schoenfelder S, Ferreira L, Wingett SW, Andrews S, Grey W, Ewels PA, et al. 2015. Mapping long-range promoter contacts in human cells with high-resolution capture Hi-C. *Nat Genet* **47:** 598–606. doi:10.1038/ng.3286
Mumbach MR, Rubin AJ, Flynn RA, Dai C, Khavari PA, Greenleaf WJ, Chang HY. 2016. HiChIP: efficient and sensitive analysis of protein-directed genome architecture. *Nat Methods* **13:** 919–922. doi:10.1038/nmeth.3999
Pertea M, Kim D, Pertea GM, Leek JT, Salzberg SL. 2016. Transcript-level expression analysis of RNA-seq experiments with HISAT, StringTie and Ballgown. *Nat Protoc* **11:** 1650–1667. doi:10.1038/nprot.2016.095
Ponnaluri VKC, Zhang G, Estève PO, Spracklin G, Sian S, Xu SY, Benoukraf T, Pradhan S. 2017. NicE-seq: high resolution open chromatin profiling. *Genome Biol* **18:** 122. doi:10.1186/s13059-017-1247-6
Quinlan AR, Hall IM. 2010. BEDTools: a flexible suite of utilities for comparing genomic features. *Bioinformatics* **26:** 841–842. doi:10.1093/bioinformatics/btq033
Ramírez F, Dündar F, Diehl S, Grüning BA, Manke T. 2014. deepTools: a flexible platform for exploring deep-sequencing data. *Nucleic Acids Res* **42:** W187–W191. doi:10.1093/nar/gku365
Ramírez F, Bhardwaj V, Arrigoni L, Lam KC, Grüning BA, Villaveces J, Habermann B, Akhtar A, Manke T. 2018. High-resolution TADs reveal DNA sequences underlying genome organization in flies. *Nat Commun* **9:** 189. doi:10.1038/s41467-017-02525-w
Rao SS, Huntley MH, Durand NC, Stamenova EK, Bochkov ID, Robinson JT, Sanborn AL, Machol I, Omer AD, Lander ES, et al. 2014. A 3D map of the human genome at kilobase resolution reveals principles of chromatin looping. *Cell* **159:** 1665–1680. doi:10.1016/j.cell.2014.11.021
Servant N, Varoquaux N, Lajoie BR, Viara E, Chen CJ, Vert JP, Heard E, Dekker J, Barillot E. 2015. HiC-Pro: an optimized and flexible pipeline for Hi-C data processing. *Genome Biol* **16:** 259. doi:10.1186/s13059-015-0831-x
Song L, Crawford GE. 2010. DNase-seq: a high-resolution technique for mapping active gene regulatory elements across the genome from mammalian cells. *Cold Spring Harb Protoc* **2010:** pdb.prot5384. doi:10.1101/pdb.prot5384
Takemon Y, Chick JM, Gerdes Gyuricza I, Skelly DA, Devuyst O, Gygi SP, Churchill GA, Korstanje R. 2021. Proteomic and transcriptomic profiling reveal different aspects of aging in the kidney. *eLife* **10:** e62585. doi:10.7554/eLife.62585
Weintraub AS, Li CH, Zamudio AV, Sigova AA, Hannett NM, Day DS, Abraham BJ, Cohen MA, Nabet B, Buckley DL, et al. 2017. YY1 is a structural regulator of enhancer-promoter loops. *Cell* **171:** 1573–1588 e1528. doi:10.1016/j.cell.2017.11.008
Yang T, Zhang F, Yardimci GG, Song F, Hardison RC, Noble WS, Yue F, Li Q. 2017. HiCRep: assessing the reproducibility of Hi-C data using a stratum-adjusted correlation coefficient. *Genome Res* **27:** 1939–1949. doi:10.1101/gr.220640.117
Zhang Y, Liu T, Meyer CA, Eeckhoute J, Johnson DS, Bernstein BE, Nusbaum C, Myers RM, Brown M, Li W, et al. 2008. Model-based Analysis of ChIP-Seq (MACS). *Genome Biol* **9:** R137. doi:10.1186/gb-2008-9-9-r137

Received August 10, 2021; accepted in revised form January 25, 2022.